Microchimica Acta (2019) 186: 275
https://doi.org/10.1007/s00604-019-3393-x

ORIGINAL PAPER

Photoelectrochemical aptamer-based sensing of the vascular endothelial growth factor by adjusting the light harvesting efficiency of g-C_3N_4 via porous carbon spheres

Ya-Ling Liu[1] · Hui-Mei Da[1] · Ya-Qin Chai[1] · Ruo Yuan[1] · Hong-Yan Liu[1]

Received: 10 December 2018 / Accepted: 29 March 2019 / Published online: 10 April 2019

Abstract

A "signal-off" sensor is described for sensitive photoelectrochemical (PEC) determination of the vascular endothelial growth factor ($VEGF_{165}$). Graphitic carbon nitride (g-C_3N_4) is used as the signalling material, and porous carbon spheres as efficient quenchers of the photocurrent. The quenching efficiency of carbon spheres is the result of two effects, viz. (a) the competitive light absorption and (b) competitive electron donor activity which decreases the number of light-generated electrons and holes and also reduces the charge separation efficiency. This new mechanism differs from the previous quenching mechanisms which usually are based on the suppression of electron transport or steric hindrance. A glassy carbon electrode was modified with an aptamer against $VEGF_{165}$. On binding of analyte ($VEGF_{165}$), the reduction of current is measured (at a typical potential of 0 V) using H_2O_2 as the electrochemical probe. The sensor has a linear response in the 10^{-5} nM to 10^2 nM $VEGF_{165}$ concentration range, and the detection limit is 3 fM.

Keywords Photoelectrochemical biosensor · Light absorption · Porous carbon spheres · Vascular endothelial growth factor

Introduction

Photoelectrochemical (PEC) assays have attractive advantages such as low cost, simple instrumentation and high sensitivity [1–6]. The PEC process refers to the conversion of photon-to-current which is caused by the electron excitation and subsequent charge transfer of a photoactive material after absorbing photons under illumination [1, 7]. For the construction of PEC biosensor, "signal-off" type was a classic photocurrent signal response pattern [7, 8]. In general, a quencher with high quenching efficiency for the initial photocurrent was necessary in "signal-off" model PEC biosensor [9, 10]. The reported photocurrent quenchers are usually materials with poor conductivity which can enhance the steric hindrance and suppress the electron transfer [4]. However, the quenching efficiency was very limited and needed further improvement. Therefore, it is meaningful to find other approach to regulate the photocurrent signal. As well known, photo-absorption was very important in a PEC process [11]. The intensity of the photocurrent signal can be tuned by adjusting the light harvesting efficiency of the photoelectric material. Therefore, it is possible to develop PEC biosensor based on the change of photo-absorption efficiency induced by light-absorption materials. Regrettably, until now, this kind of materials has been rarely reported.

Carbon nanomaterials have attracted much attention due to their wide range of applications, such as biological imaging [12], green processing [13], and thin film transistors [14–16], originated from their advantages of excellent chemical stability, electrical and optical properties [17]. Despite they are widely applied in these area, exploiting them with high light absorption efficiency is just beginning [18, 19]. Since carbon nanomaterial exhibited high surface area, excellent dispersity, and good light absorption efficiency, it was a good candidate for photocurrent signal quencher in PEC assay and was expected to be an effective signal quencher.

Electronic supplementary material The online version of this article (https://doi.org/10.1007/s00604-019-3393-x) contains supplementary material, which is available to authorized users.

✉ Ruo Yuan
yuanruo@swu.edu.cn

✉ Hong-Yan Liu
liuhy860@swu.edu.cn

[1] Key Laboratory of Luminescent and Real-Time Analytical Chemistry (Southwest University), Ministry of Education, College of Chemistry and Chemical Engineering, Southwest University, Chongqing 400715, People's Republic of China

The vascular endothelial growth factor (VEGF) is a kind of cell product which simulates the formation of new blood vessels of tissues [20–22]. The abnormal expression of VEGF is closely related to many diseases [23]. Therefore, the sensitive detection of $VEGF_{165}$ can be a promising approach in clinical diagnoses. To date, there are various analytical methods for detecting $VEGF_{165}$, such as field-effect transistor (FET) [24], fluorescence (FL) [22] and electrochemical [25], enzyme-linked immunosorbent assay (ELISA) [26]. However, the analytical methods are complicated operation, high cost and time-consuming. Lately, the aptasensors on 2D nanomaterial have attracted much attention due to their excellent property, such as stability, specificity and easy operation [27, 28]. Herein, we proposed a novel "signal-off" PEC biosensor for the detection of $VEGF_{165}$ by using g-C_3N_4 as the signal indicator and porous carbon spheres as the efficient signal quencher. As shown in Scheme 1, photoactive material g-C_3N_4 can be filmed on the bare electrode surface, which provided a high initial PEC signal. The DNA strand S_0 and S_1 are two split parts of a whole $VEGF_{165}$ aptamer [7, 29]. Firstly, S_0 was incubated on the electrode, when target $VEGF_{165}$ and S_1 modified porous carbon spheres were incubated on the electrode, a sandwich structure can be fabricated by specific recognition of the aptamer and $VEGF_{165}$ to form aptamer-$VEGF_{165}$ complex, thus the carbon material got close to the electrode. Therefore, the original photocurrent signal was efficiently quenched by porous carbon spheres via competing with g-C_3N_4 to absorb light and competing electron donors to reduce the separation efficiency of electron and hole, as depicted in Scheme 1c. The change of the photocurrent should be related to the concentration of $VEGF_{165}$, which was used for the detection of target $VEGF_{165}$. The "signal-off" method based on adjusting the light absorption efficiency will provide new direction for design of other PEC biosensors.

Experimental section

Materials and reagents

Polyacrylic acid (PAA) was purchased from Sigma-Aldrich (Beijing, China, www.jk-scientific.com). hydrogen peroxide (H_2O_2) was bought from Kelong Chemical Inc. (Chengdu, China, webmaster53029.company.lookchem.cn). N-(3-(Dimethylamino)propyl)-N′-ethylcarbodiimide hydrochloride (EDC), N-hydroxy succinimide (NHS), gold chloride ($HAuCl_4$), hexanethiol (HT), cetyltrimethyl-ammonium bromide

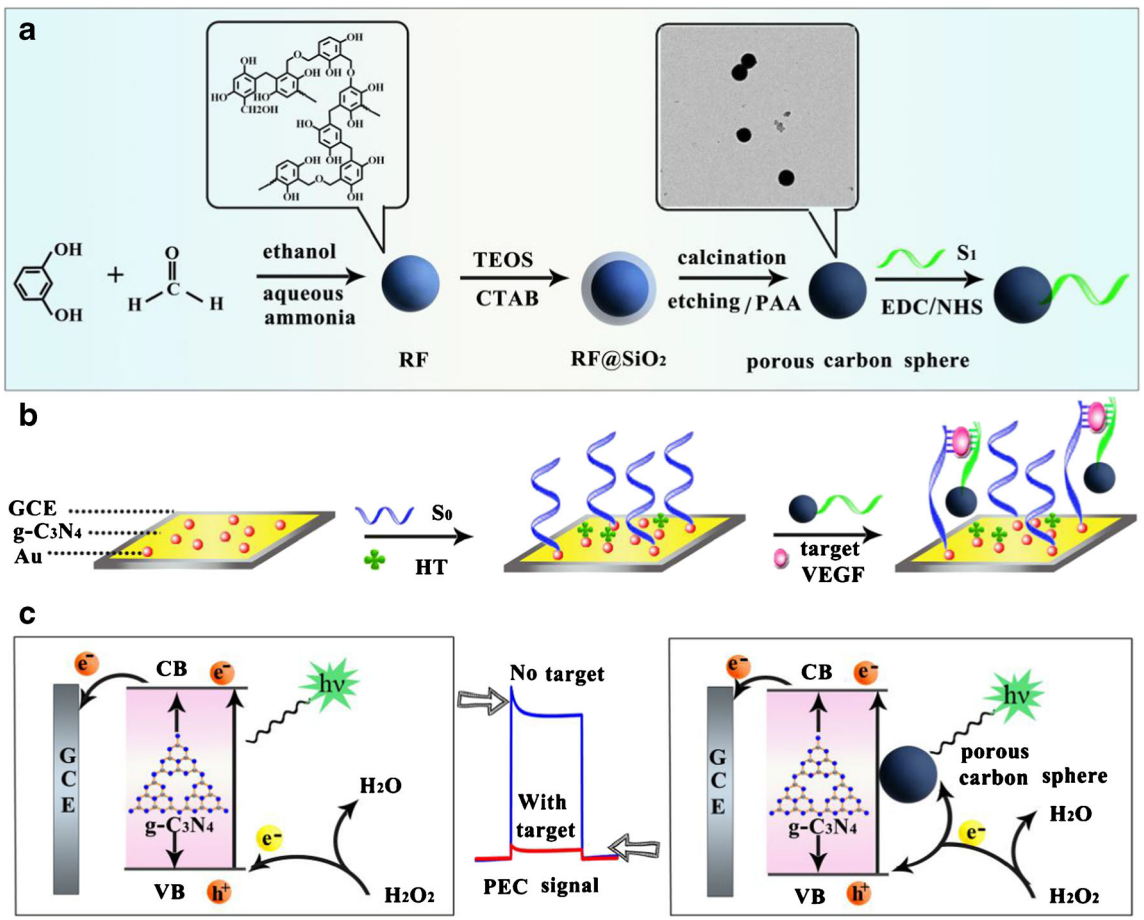

Scheme 1 **a** Preparation and modification of porous carbon spheres; (**b**) Schematic illustration for the preparation of PEC biosensor, (**c**) The mechanism of the photocurrent response in graphitic carbon nitride

(CTAB, 98%), ammonium hydroxide ($NH_3 \cdot H_2O$, 28% by weight in water), poly(vinyl pyrrolidone) (PVP, Mw~40,000), tetraethyl orthosilicate (TEOS, 99%), resorcinol, ethanol, formaldehyde (37%) and tetrabutyl orthotitanate (TBOT, 99%) were obtained from Sigma-Aldrich (St. Louis, MO, USA, www.sigmaaldrich. com). 0.1 M Na_2HPO_4, 0.1 M KCl and 0.1 M KH_2PO_4 were dissolving to obtain phosphate buffered saline (PBS, pH 7.0). Potassium ferrocyanide and potassium ferricyanide were dissolving with 0.1 M PBS solution (pH 7.0) to prepare $[Fe(CN)_6]^{3-/4-}$ solution (5.0 mM). Vascular endothelial growth factor ($VEGF_{165}$) and the oligonucleotides in this work were ordered from Sangon Inc. (Shanghai, China, www. sangon. com), which were shown as follows:

S_0: 5'-AAGAGTGCAGGGTTTTTTTTT-SH-3'
S_1: 5'-NH_2-ACCGTCTTCCAGAC-3'

Instrumentation

The PEC workstation (Ivium, P Netherlands) was used for PEC measurement, which contained a three-electrode system: the glassy carbon electrode was the working electrode, platinum wire electrode was the counter electrode, and Ag/AgCl (saturated KCl) electrode was the reference electrode. The CHI660D electrochemical workstation (Shanghai Chenhua Instrument, Shanghai, China) was used for cyclic voltammetry (CV) and electrochemical impedance spectroscopy (EIS) detection. The characterization of the synthesized carbon materials was obtained from transmission electron microscope (TEM, HT7700, Hitachi, Japan).

Synthesis of graphitic carbon nitride (g-C_3N_4)

The g-C_3N_4 was obtained based on previously reported literature with some modifications [30, 31]. First, 15 g of urea was dried in a crucible at 80 °C and held for 12 h, next, the dried sample was calcined at 550 °C for 4 h using a heating rate of 10 °C min^{-1} in a muffle furnace. The powders were with slight yellow color.

Preparation of porous carbon spheres

Porous carbon spheres were prepared as follows (Scheme 1a), firstly, the resorcinol-formaldehyde (RF) spheres were synthesized by mixing formaldehyde solution (0.07 mL), aqueous ammonia solution (28%, 0.05 mL), deionized water (10 mL), resorcinol (0.05 g) and ethanol (4 mL), which were stirred for 12 h to get the RF sample by centrifuging out, washing three times with ethanol, and redispersing in 10 mL of ethanol [32, 33]. The above RF particles were then treated with cetyltrimethyl ammonium bromide (CTAB, 5 mg·mL^{-1}) for allowing CTAB adsorption on the surface of RF spheres. The above particles were then centrifuged to separate from the solution, and redispersed in ethanol (16 mL). The solution was mixed with water (32 mL), 0.4 mL of ammonia (28%). After stirring for 30 min, TEOS (0.8 mL) was added and stirring overnight. The resulting RF@SiO_2 core-shell composites were centrifuged by washing with ethanol for three times and dried in a vacuum. To obtain the C@SiO_2, the dried RF@SiO_2 samples were heated at 800 °C in N_2 with a heating rate of 2.5 °C min^{-1} for 2 h and then cooled to room temperature. Finally, to prepare the porous carbon spheres, 100 mg of the sample were dispersed in 30 mL of the aqueous NaOH solution (5 M), following by stirring for 5 h at 80 °C to etching the SiO_2 layer. Then, the porous carbon spheres samples were centrifuged and washed with ethanol and ultrapure water for several times, followed by dispersal in ultrapure water.

Preparation of S_1 modified porous carbon spheres

The porous carbon spheres were modified by polyacrylic acid (PAA). Firstly, 1 mL of the samples was acidified with 0.072 g PAA in 10 mL water by stirring overnight. The product was then tcentrifuged three times and redispersed in ultrapure water.

The S_1 modified porous carbon spheres composite was obtained as follows: Firstly, 500 μL of porous carbon spheres was dissolved in 500 μL of PBS. Next, 0.0388 g EDC and 0.0058 g NHS dissolved in 1 mL PBS solution (PH 7.0), then the solution were dropped to the mixture and stirred for 1 h for activating the carboxyl group on the porous carbon spheres. 20 μL of S_1 (50 μM) was then added to the mixture solution, stirring for 4 h to obtain S_1 modified porous carbon spheres, the product was washed and redispersed in PBS solution (1 mL, pH 7.0).

Fabrication of the PEC biosensor

Scheme 1b represented the stepwise fabrication process for the biosensor. First of all, the glassy carbon electrode (GCE) (Φ = 4 mm) was sonicated in ultrapure water and anhydrous ethanol for three times after polished with alumina powder and dried at room temperature for 10 min. 10 μL solution of g-C_3N_4 (1 mg·mL^{-1}) was dropped onto the GCE to form a homogeneous film after drying for 1 h. Next, Au NPs were electrodeposited on GCE by using $HAuCl_4$ (1%) solution under −0.2 V for 10 s. After that, 10 μL of 2.0 μM S_0 was coated on the electrode to incubate at 4 °C for 12 h. After blocking the nonspecific adsorption sites with HT (1.0 mM) for 40 min, $VEGF_{165}$ and S_1 modified porous carbon spheres solution were incubated on the electrode to hybridize with the S_0 for 2 h at 37 °C. The electrode should be rinsed with ultrapure water after each step.

PEC measurement

The PEC measurement was carried out under optimal experimental conditions of 5 mL 0.1 M PBS solution (PH = 7.0) containing 0.1 M electron donor H_2O_2, the light-emitting diode (LED) light source acted as excitation light source with switching off-on-off for 10–20-10 s under the potential of 0.0 V.

Cyclic voltammetry (CV) and electrochemical impedance spectroscopy (EIS)

The CV measurement was recorded in 0.1 M PBS solution (pH = 7.0), which contained 5.0 mM $[Fe(CN)_6]^{3-/4-}$ at the potential between −0.2 V and 0.6 V, with a scan rate of 50 $mV{\cdot}s^{-1}$. And the EIS measurement was performed in 0.1 M PBS solution (PH = 7.0) containing 5.0 mM $[Fe(CN)_6]^{3-/4-}$, with a scan rate of 100 $mV{\cdot}s^{-1}$.

Results and discussion

Morphology and characterization of porous carbon spheres

To obtain carbon materials with good dispersion and facilitate the DNA modification, the carbon spheres were obtained by a protected calcination procedure (Scheme 1a), which involved the synthesis of RF core and coating of the cores with porous SiO_2 layer, followed by the protected calcination procedure and selective etching the SiO_2 layer by NaOH solution. The morphology of the C@SiO_2 and porous carbon spheres was characterized by TEM. As presented in Fig. 1a ,c, the C@SiO_2 exhibits regular spherical structures with a uniform size. After removing the outer SiO_2 layer by aqueous NaOH, the sample shows a porous structure with the size of 540 ± 39 nm (Fig. 1b and d). The surface area of the carbon spheres is 345 $m^2{\cdot}g^{-1}$ (Fig. S-1), implying that the carbonization of RF resulted a mesoporous structure.

Quenching mechanism of the porous carbon spheres

To investigate the quenching mechanism, the quenching efficiency of the porous carbon spheres was adjusted to be similar to C@SiO_2. As evaluated by PEC, the decreases of photocurrent (ΔI) caused by porous carbon spheres and C@SiO_2 are 1.319 μA and 1.407 μA, respectively (Fig. 2a and Fig. S2A). Cyclic voltammograms (CV) and electrochemical impedance spectroscopy (EIS) of g-C_3N_4, g-C_3N_4/C@SiO_2 and g-C_3N_4/porous carbon spheres were then measured to compare the quenching mechanism. The voltammetric results confirm that when g-C_3N_4 immobilized on GCE, there is a well-defined redox peak (Fig. S2B and Fig. 2b). A significant decline can be obtained when C@SiO_2 nanomaterials are further modified on the electrode (curve b in Fig. S2B). This is ascribed to the inhibition of electron transfer by the SiO_2 layer. The conductivity is further investigated by EIS detection. As shown in Fig. S2C, the nyquist plots reveal a remarkable increase in the charge-transfer resistance (R_{et}) from g-C_3N_4 (curve a) to g-C_3N_4/C@SiO_2 (curve b), which indicates an increase in reaction resistance. However, an increase of the redox peak is found after porous carbon spheres immobilized on the g-

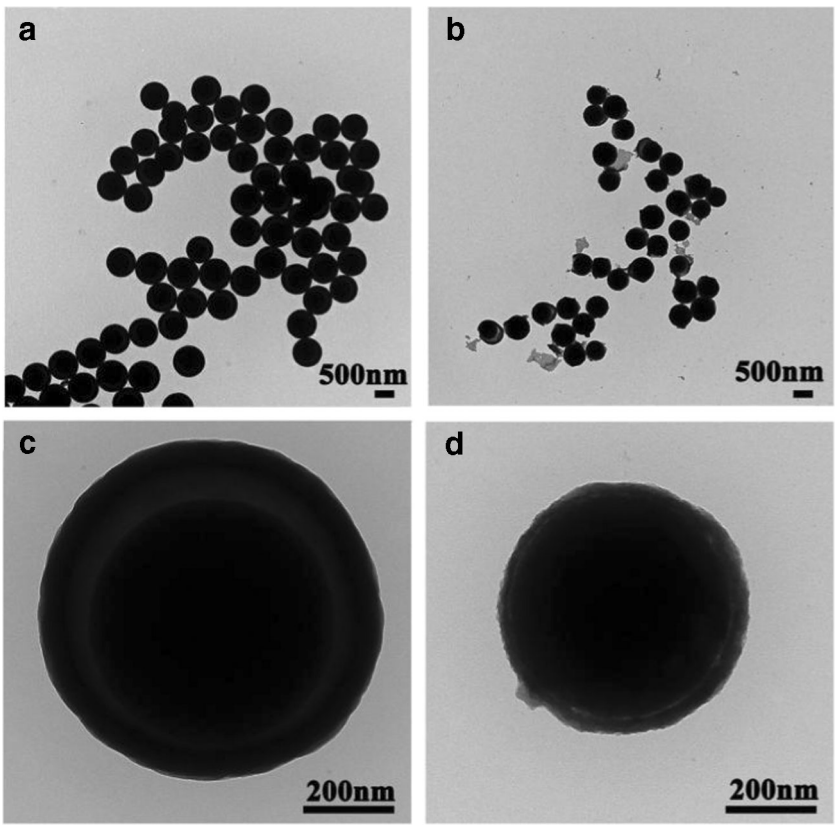

Fig. 1 TEM images of C@SiO_2 (**a**, **c**) and porous carbon spheres (**b**, **d**)

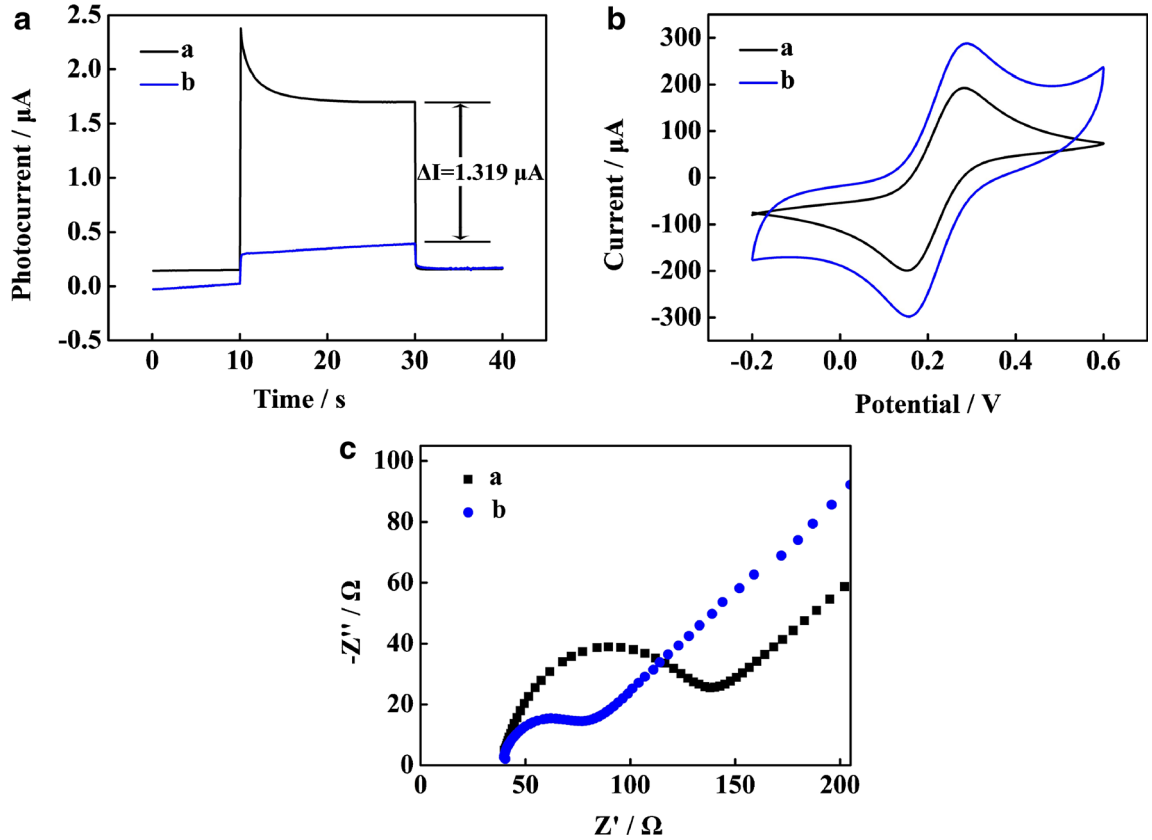

Fig. 2 **a** The PEC responses of (a) g-C_3N_4 and (b) g-C_3N_4/porous carbon sphere with 365 nm irradiation in 0.1 M pH 7.0 PBS containing 0.1 M H_2O_2. (**b**) CV of (a) g-C_3N_4 and (b) g-C_3N_4/porous carbon sphere in 0.1 M pH 7.0 PBS solution containing 5.0 mM $[Fe(CN)_6]^{3-/4-}$ at the potential between −0.2 V and 0.6 V. (**c**) Nyquist diagrams for (a) g-C_3N_4 and (b) g-C_3N_4/porous carbon sphere modified GCE in 0.1 M pH 7.0 PBS containing 5.0 mM $[Fe(CN)_6]^{3-/4-}$

C_3N_4 electrode (curve b, Fig. 2b), owing to the conductivity of the porous carbon spheres. Similarly, compared to the R_{et} of g-C_3N_4 (curve a), a decrease of the R_{et} is obtained after the modification of porous carbon spheres (curve b, Fig. 2c). This is due to the accelerated electron transfer caused by carbon spheres. These results strongly supported the idea that carbon spheres were electroconductive material which can quench the photocurrent signal due to the competitive light absorption and competitive electron donors, which decreased the light generated electrons and holes from g-C_3N_4 and also reduced the charge separation efficiency.

Photoelectrochemical and electrochemical characterization of the modified electrode

The construction of the biosensor was investigated by PEC and CV measurements. The PEC characterization of the stepwise-modified electrode is shown in Fig. 3a, there is nearly no photocurrent of the bare GCE (curve a), obviously photocurrent response is observed when g-C_3N_4 was coated onto the bare GCE, which provided a high initial PEC photocurrent signal (curve b). Subsequently, a further enhancement of photocurrent was obtained after Au NPs was modified on the electrode (curve c), because the Au NPs facilitated the electron transfer. After incubating with S_0 and HT, the photocurrent decreased, which was probably caused by the poor charge transfer ability (curve d and curve e). Finally, with the immobilization of $VEGF_{165}$ and S_1 modified porous carbon spheres, the photocurrent decreased significantly according to the reduced light absorption induced by porous carbon spheres.

CV was investigated to characterize the step-by-step construction process of the modified electrode. As exhibited in Fig. 3b, a well redox peak of the bare GCE was observed (curve a). The peak current apparently decreased when g-C_3N_4 was modified on the GCE (curve b). After electrodepositing with Au NPs, the peak current increased (curve c), because Au NPs possessed well conductivity. The redox peak declined after incubating with S_0 (curve d), which was attributed to that DNA with negative charge hindered the electron transfer. Subsequently, the peak current further decreased (curve e) after blocking with HT, owing to that HT greatly reduced the electronic transmission. Subsequently, there was an enhancement of the redox peak after S_1 modified porous carbon spheres and $VEGF_{165}$ were assembled onto the electrode (curve f), which confirmed the excellent electrical conductivity of the porous carbon spheres.

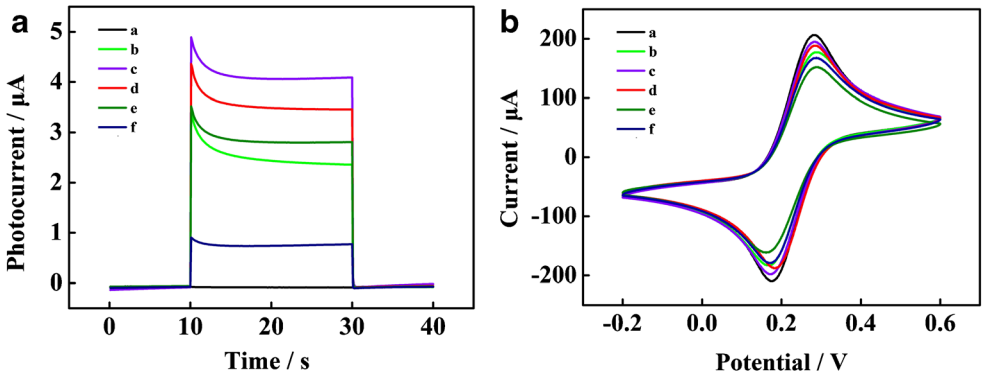

Fig. 3 **a** PEC responses of (a) GCE, (b) g-C_3N_4/GCE, (c) AuNPs/g-C_3N_4/GCE, (d) S_0/AuNPs/g-C_3N_4/GCE, (e) HT/S_0/AuNPs/g-C_3N_4/GCE, (f) S_1-carbon/target $VEGF_{165}$/HT/S_0/AuNPs/g-C_3N_4/GCE with 365 nm irradiation in 0.1 M pH 7.0 PBS containing 0.1 M H_2O_2. (**b**) CV responses of (a) GCE, (b) g-C_3N_4/GCE, (c) AuNPs/g-C_3N_4/GCE, (d) S_0/AuNPs/g-C_3N_4/GCE, (e) HT/S_0/AuNPs/g-C_3N_4/GCE, (f) S_1-carbon/target $VEGF_{165}$/HT/S_0/AuNPs/g-C_3N_4/GCE in 0.1 M pH 7.0 PBS containing 5.0 mM $[Fe(CN)_6]^{3-/4-}$ at the potential between −0.2 V and 0.6 V

Analytical performance of the biosensor for $VEGF_{165}$ detection

The assembled PEC aptasensor was applied for determination of $VEGF_{165}$ as a model. $VEGF_{165}$ with various concentrations was detected. As exhibited in Fig. 4, the calibration plot shows a nice linear relationship between the decrease of photocurrent (ΔI) and the logarithm of the $VEGF_{165}$ concentration from 10^{-5} nM to 10^2 nM with the detection limit of 3 fM. The linear equation for $VEGF_{165}$ detection is $\Delta I = 0.1920\lg c + 2.739$, where c is the concentration of $VEGF_{165}$, with a correlation coefficient of 0.9939. Besides, a comparison of the analytical performance between the PEC biosensor and the previous reported methods was shown in Table 1, it can be observed that the "signal-off" PEC biosensor displays wider linear range and higher sensitivity compared to the reported methods, showing an excellent analytical performance.

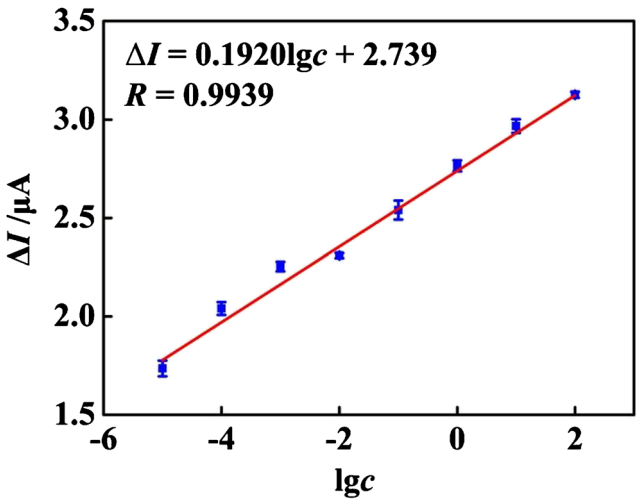

Fig. 4 The linear relationship between the change of photocurrent and the concentration of $VEGF_{165}$ from10^{-5} nM to 10^2 nM

Selectivity and stability of the PEC biosensor

In order to investigate the specificity of the PEC biosensor, alpha-fetal protein (AFP), carcinoembryonic antigen (CEA), bovine serum albumin (BSA) and prostate specific antigen (PSA) were chosen as the interfering agents. As shown in Fig. 5a, there is an obvious photocurrent decrease (ΔI = 2.041 μA) with the addition of 100 fM $VEGF_{165}$. However, there are negligible photocurrent changes with the addition of 1 pM AFP, CEA, BSA and PSA (ΔI = 0.362 μA, 0.469 μA, 0.310 μA, 0.593 μA). The result confirmed that the PEC biosensor displayed high specificity to $VEGF_{165}$. Moreover, the stability was investigated by continuous cyclic measuring for 10 cycles under continuous off-on-off light. As shown in Fig. 5b, the constructed PEC biosensor shows negligible photocurrent decay in cyclic experiments, with RSD of 1.87%, indicating good stability for the biosensor.

Table 1 Comparison for $VEGF_{165}$ detection between our proposal method and other reported detection methodologies

Analytical method	Linear range	Detection limit	Ref.
luminescence	50 pM~2000 pM	6 pM	[34]
optical	0~1 nM	50 pM	[35]
FL	10 nM~80 nM	1.3 nM	[36]
CL	0~15 nM	50 pM	[37]
electrochemical	50 pM~150 pM	50 pM	[38]
ECL	10 fM~10 nM	10 fM	[39]
PEC	100 fM~10 nM	30 fM	[7]
PEC	10 fM~100 nM	3 fM	our work

Abbreviations: fluorescence (FL); chemiluminescence (CL); electrochemiluminescent (ECL)

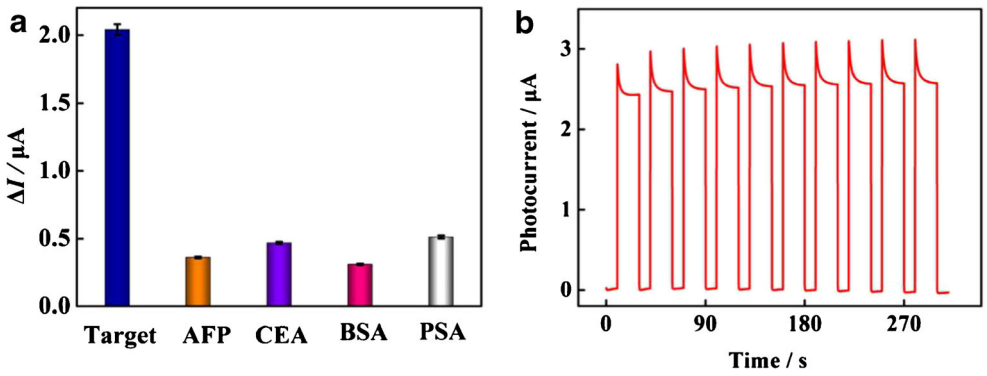

Fig. 5 **a** Selectivity of the PEC biosensor with interferences: AFP, CEA, BSA, and PSA. **b** Stability of this PEC biosensor incubated with 1 pM $VEGF_{165}$ under continuous off-on-off light for 10 cycles

Analysis of clinical serum samples

To research the potential application of the PEC aptasensor, the human blood serum samples (provided by the Ninth People's Hospital of Chongqing, China) were used for research the spiked recovery experiment. Firstly, the serum samples were diluted 10 times with 0.1 M PBS (pH 7.0). The target $VEGF_{165}$ was diluted with serum samples to different concentrations for further detection. The recovery rate of $VEGF_{165}$ was between 87.30% and 107.47%, as shown in Table S-1, suggesting that the PEC aptasensor exhibits great potential for real sample analysis.

Conclusions

We show in this work a construction of a novel "signal-off" biosensor by using g-C_3N_4 as signal indicator and porous carbon spheres as signal quencher. The biosensor displayed higher sensitivity and wider linear range for the detection of $VEGF_{165}$. The photocurrent of g-C_3N_4 is quenched due to the superior light absorption capacity of porous carbon spheres. This is different from previously reported quenching mechanisms. We are able to confirm that tuning the light absorption is an effective method to regulate photocurrent in the construction of PEC biosensor. We also believe that the "signal-off" strategy developed here can provide a promising platform and offer more opportunities for producing other biosensors with further enhanced performance.

Acknowledgements This work was financially supported by the National Natural Science Foundation of China (Grant Nos. 21501081, 21675129, 51473136, and 21775124) and the Fundamental Research Funds for the Central Universities (XDJK2017C021, XDJK2018AA003).

Compliance with ethical standards The author(s) declare that they have no competing interests.

References

1. Zhao WW, Xu JJ, Chen HY (2015) Photoelectrochemical bioanalysis: the state of the art. Chem Soc Rev 44:729–741
2. Chu YX, Deng AP, Wang WJ, Zhu JJ (2019) Concatenated catalytic hairpin assembly/Hyperbranched hybridization chain reaction based enzyme-free signal amplification for the sensitive Photoelectrochemical detection of human telomerase RNA. Anal Chem 91:3619–3627
3. Cheng WJ, Pan JH, Yang JY, Zheng ZY, Lu FS, Chen YW, Gao WH (2018) A photoelectrochemical aptasensor for thrombin based on the use of carbon quantum dot-sensitized TiO_2 and visible-light photoelectrochemical activity. Microchim Acta 185:263
4. Zheng YN, Liang WB, Xiong CY, Yuan YL, Chai YQ, Yuan R (2016) Self-enhanced ultrasensitive Photoelectrochemical biosensor based on Nanocapsule packaging both donor-acceptor-type photoactive material and its sensitizer. Anal Chem 88:8698–8705
5. Qin CD, Bai X, Zhang Y, Gao K (2018) Photoelectrochemical CdSe/TiO_2 nanotube array microsensor for high-resolution in-situ detection of dopamine. Microchim Acta 185:278
6. Zhou YL, Sui CJ, Yin HS, Wang Y, Wang MH, Ai SY (2018) Tungsten disulfide (WS_2) nanosheet-based photoelectrochemical aptasensing of chloramphenicol. Microchim Acta 185:453
7. Da HM, Liu HY, Zheng YN, Yuan R, Chai YQ (2018) A highly sensitive $VEGF_{165}$ photoelectrochemical biosensor fabricated by assembly of aptamer bridged DNA networks. Biosens Bioelectron 101:213–218
8. Yan K, Liu Y, Yang YH, Zhang JD (2015) A cathodic "signal-off" Photoelectrochemical Aptasensor for ultrasensitive and selective detection of Oxytetracycline. Anal Chem 87:12215–12220
9. Li MJ, Zheng YN, Liang WB, Yuan R, Chai YQ (2017) Using p-type PbS quantum dots to quench photocurrent of fullerene-au NP@MoS_2 composite structure for ultrasensitive Photoelectrochemical detection of ATP. ACS Appl Mater Interfaces 9:42111–42120
10. Li MJ, Zheng YN, Liang WB, Yuan YL, Chai YQ, Yuan R (2016) An ultrasensitive "on-off-on" photoelectrochemical aptasensor based on signal amplification of a fullerene/CdTe quantum dots sensitized structure and efficient quenching by manganese porphyrin. Chem Commun 52:8138–8141
11. Fan GC, Zhu H, Du D, Zhang JR, Zhu JJ, Lin YH (2016) Enhanced Photoelectrochemical Immunosensing platform based on CdSeTe@CdS:Mn Core-Shell quantum dots-sensitized TiO_2 amplified by CuS nanocrystals conjugated signal antibodies. Anal Chem 88:3392–3399
12. Hong GS, Diao S, Antaris AL, Dai HJ (2015) Carbon nanomaterials for biological imaging and Nanomedicinal therapy. Chem Rev 115:10816–10906

13. Kawamoto M, He P, Ito Y (2017) Green processing of carbon nanomaterials. Adv Mater 29:1602423
14. Cao CY, Andrews JB, Kumar A, Franklin AD (2016) Improving contact interfaces in fully printed carbon nanotube thin-film transistors. ACS Nano 10:5221–5229
15. Franklin AD, Luisier M, Han SJ, Tulevski G, Breslin CM, Gignac L, Lundstrom M, Haensch W (2012) Sub-10 nm carbon nanotube transistor. Nano Lett 12:758–762
16. Yang YJ, Ding L, Han J, Zhang ZY, Peng LM (2017) High-performance complementary transistors and medium-scale integrated circuits based on carbon nanotube thin films. ACS Nano 11: 4124–4132
17. Wang Z, Yu Y, Gui R, Jin H, Xia Y (2016) Carbon nanomaterials-based electrochemical aptasensors. Biosens Bioelectron 79:136–149
18. Yang ZP, Ci LJ, Bur JA, Lin SY, Ajayan PM (2008) Experimental observation of an extremely dark material made by a low-density nanotube Array. Nano Lett 8:446–451
19. Kaul AB, Coles JB, Eastwood M, Green RO, Bandaru PR (2013) Ultra-high optical absorption efficiency from the ultraviolet to the infrared using multi-walled carbon nanotube ensembles. Small 9: 1058–1065
20. Shamsipur M, Farzin L, Tabrizi MA, Molaabasi F (2015) Highly sensitive label free electrochemical detection of $VGEF_{165}$ tumor marker based on "signal off" and "signal on" strategies using an anti-$VEGF_{165}$ aptamer immobilized BSA-gold nanoclusters/ionic liquid/glassy carbon electrode. Biosens Bioelectron 74:369–375
21. Johari-Ahar M, Karami P, Ghanei M, Afkhami A, Bagheri H (2018) Development of a molecularly imprinted polymer tailored on disposable screen-printed electrodes for dual detection of EGFR and VEGF using nanoliposomal amplification strategy. Biosens Bioelectron 107:26–33
22. Moghadam FM, Rahaie M (2019) A signal-on nanobiosensor for $VEGF_{165}$ detection based on supraparticle copper nanoclusters formed on bivalent aptamer. Biosens Bioelectron 132:186–195
23. Loureiro RM, D'amore PA (2005) Transcriptional regulation of vascular endothelial growth factor in cancer. Cytokine Growth Factor Rev 16:77–89
24. Chen HC, Qiu JT, Yang FL, Liu YC, Chen MC, Tsai RY, Yang HW, Lin CY, Lin CC, Wu TS, Tu YM, Xiao MC, Ho CH, Huang CC, Lai CS, Hua MY (2014) Magnetic-composite-modified polycrystalline silicon nanowire field-effect transistor for vascular endothelial growth factor detection and Cancer diagnosis. Anal Chem 86: 9443–9450
25. Pan LH, Kuo SH, Lin TY, Lin CW, Fang PY, Yang HW (2017) An electrochemical biosensor to simultaneously detect VEGF and PSA for early prostate cancer diagnosis based on graphene oxide/ssDNA/PLLA nanoparticles. Biosens Bioelectron 89:598–605
26. Hsu MY, Chen SJ, Chen KH, Hung YC, Tsai HY, Cheng CM (2015) Monitoring VEGF levels with low-volume sampling in major vision-threatening diseases: age-related macular degeneration and diabetic retinopathy. Lab Chip 15:2357–2363
27. Xiong MY, Rong QM, Meng HM, Zhang XB (2017) Two-dimensional graphitic carbon nitride nanosheets for biosensing applications. Biosens Bioelectron 89:212–223
28. Zhao XH, Kong RM, Zhang XB, Meng HM, Liu WN, Tan WH, Shen GL, Yu RQ (2011) GrapheneDNAzyme based biosensor for amplified fluorescence "turn-on" detection of Pb^{2+} with a high selectivity. Anal Chem 83:5062–5066
29. Liao WC, Sohn YS, Riutin M, Cecconello A, Parak WJ, Nechushtai R, Willner I (2016) The application of stimuli-responsive VEGF- and ATP-aptamer-based microcapsules for the controlled release of an anticancer drug, and the selective targeted cytotoxicity toward Cancer cells. Adv Funct Mater 26:4262–4273
30. Yu HJ, Shi R, Zhao YX, Bian T, Zhao YF, Zhou C, Waterhouse GIN, Wu LZ, Tung CH, Zhang TR (2017) Alkali-assisted synthesis of nitrogen deficient graphitic carbon nitride with tunable band structures for efficient visible-light-driven hydrogen evolution. Adv Mater 29:1605148
31. Cao HX, Wang L, Pan CG, He YS, Liang GX (2018) Aptamer based electrochemiluminescent determination of bisphenol a by using carboxylated graphitic carbon nitride. Microchim Acta 185:463
32. Liu J, Qiao SZ, Liu H, Chen J, Orpe A, Zhao DY, Lu GQ (2011) Extension of the Stöber method to the preparation of monodisperse resorcinol-formaldehyde resin polymer and carbon spheres. Angew Chem Int Ed 50:5947–5951
33. Liu HY, Joo JB, Dahl M, Fu LS, Zeng ZZ, Yin YD (2015) Crystallinity control of TiO_2 hollow shells through resin-protected calcination for enhanced photocatalytic activity. Energy Environ Sci 8:286–296
34. Lan JN, Li L, Liu YX, Yan L, Li CY, Chen JH, Chen XS (2016) Upconversion luminescence assay for the detection of the vascular endothelial growth factor, a biomarker for breast cancer. Microchim Acta 183:3201–3208
35. Freeman R, Girsh J, Jou AFJ, Ho JAA, Ja H, Dernedde J, Willner I (2012) Optical Aptasensors for the analysis of the vascular endothelial growth factor (VEGF). Anal Chem 84:6192–6198
36. Cao Y, Wang ZH, Cao JP, Mao XX, Chen GF, Zhao J (2017) A general protein aptasensing strategy based on untemplated nucleic acid elongation and the use of fluorescent copper nanoparticles: application to the detection of thrombin and the vascular endothelial growth factor. Microchim Acta 184:3697–3704
37. Li WY, Zhang QF, Zhou HP, Chen J, Li YX, Zhang CY, Yu C (2015) Chemiluminescence detection of a protein through the aptamer-controlled catalysis of a porphyrin probe. Anal Chem 87: 8336–8341
38. Zhao S, Yang WW, Lai RY (2011) A folding-based electrochemical aptasensor for detection of vascular endothelial growth factor in human whole blood. Biosens Bioelectron 26:2442–2447
39. Zhang H, Li MX, Li CH, Guo ZH, Dong HL, Wu P, Cai CX (2015) G-quadruplex DNAzyme-based electrochemiluminescence biosensing strategy for $VEGF_{165}$ detection: combination of aptamer-target recognition and T7 exonuclease-assisted cycling signal amplification. Biosens Bioelectron 74:98–103